

Self-supervised Egomotion and Depth Learning via Bi-directional Coarse-to-Fine Scale Recovery

Hao Qu, Lilian Zhang, Xiaoping Hu, Xiaofeng He, Xianfei Pan, Changhao Chen*

Abstract—Self-supervised learning of egomotion and depth has recently attracted great attentions. These learning models can provide pose and depth maps to support navigation and perception task for autonomous driving and robots, while they do not require high-precision ground-truth labels to train the networks. However, monocular vision based methods suffer from pose scale-ambiguity problem, so that can not generate physical meaningful trajectory, and thus their applications are limited in real-world. We propose a novel self-learning deep neural network framework that can learn to estimate egomotion and depths with absolute metric scale from monocular images. Coarse depth scale is recovered via comparing point cloud data against a pretrained model that ensures the consistency of photometric loss. The scale-ambiguity problem is solved by introducing a novel two-stages coarse-to-fine scale recovery strategy that jointly refines coarse poses and depths. Our model successfully produces pose and depth estimates in global scale-metric, even in low-light condition, i.e. driving at night. The evaluation on the public datasets demonstrates that our model outperforms both representative traditional and learning based VOs and VIOs, e.g. VINS-mono, ORB-SLAM, SC-Learner, and UnVIO.

Index Terms—Visual Odometry, Depth Learning, Visual-inertial Odometry, Deep Neural Network

I. INTRODUCTION

EGOMOTION and scene perception plays a vital role in autonomous systems. Self-driving and mobile robots are normally equipped with a combination of sensors, e.g. camera, inertial measurement unit (IMU) and LIDAR, for self-motion and scene perception, which further supports path planning and decision making.

A representative method is visual odometry (VO), which tracks and matches visual features between consecutive images, and establishes multi-view geometry model to calculate relative pose. However, pose estimates from monocular VO are scale-ambiguous. Stereo VO exploits stereo camera to recover the absolute scale of pose estimates, and is generally more robust because of information fusion from two cameras. Visual-inertial odometry (VIO) attracts attentions, as it combines camera with inertial sensor to estimate system states that can recover global-scale, and improve the robustness in complex environments.

Recently, deep learning based methods construct end-to-end deep neural network model to learn pose from images directly. They can be generally categorized into supervised learning based and unsupervised learning based approaches. Supervised

learning based VO/VIOs require ground-truth pose as labels to train the neural network model. Though they show good performance in challenging scenes, e.g. in featureless areas or in complex light-conditions, labelling data is costly and time-consuming. In addition, the trained model is hard to generalize to new environments with completely different scene geometry and appearance. Thus, there are a number of attempts on unsupervised learning based VO/VIOs that can jointly learn to produce relative pose and scene depths, by constructing photometric loss between the real image and wrapped image from novel view synthesis. However, They still suffer from scale ambiguity problem.

To solve this problem, previous researchers use prior information, e.g. velocity or camera height to recover the scale metric. A recent work, i.e. VIOLearner [1], calculates the interpolated depths from pointcloud data to replace depth learning, and use the depths with absolute scale to obtain pose with absolute scale. However, the performance of scale recovery highly depends on the quality of pointcloud data, i.e. sparsity. Moreover, the interpolated depths do not conform to the multi-view geometry, and thus can be not used as supervised labels for depth learning, so that VIOLearner only produces pose estimates.

We instead propose a self-supervised learning framework to jointly estimate ego-motion and depths with global scale metric from image sequences, via a novel Bi-directional coarse-to-fine scale recovery process. Instead of interpolating depths directly, in our model, point clouds data are used to compare with a pretrained depth model to calculate coarse scale ratio and depths. A two-stages process of scale recovery is proposed to firstly produce coarse pose via a single-directional scale recovery conditioned on coarse depths, and then refine depths and poses together through a bi-directional coarse-to-fine scale recovery. Our model is capable of generating both depths and poses with global scale accurately and robustly, even in low-light conditions (i.e. driving at night). In addition, inertial data can also be introduced into the framework via an attention based fusion module that further improves the performance of rotation estimation.

Our contributions can be summarized as follows:

- We propose a novel self-supervised learning framework that can jointly estimate ego-motion and depths with global scale metric from image sequences.
- We propose a novel Bi-directional coarse-to-fine scale recovery process that jointly refines coarse poses and depths. Depth scale is recovered via comparing point cloud data against a pretrained model that ensures the consistency of photometric loss.

The authors are with the College of Intelligence Science and Technology, National University of Defense Technology, Changsha, 410073, China

*Corresponding author: Changhao Chen (changhao.chen66@outlook.com)

This work was supported by National Natural Science Foundation of China (NSFC) under the Grant Number of 62103427, 62073331, 62103430.

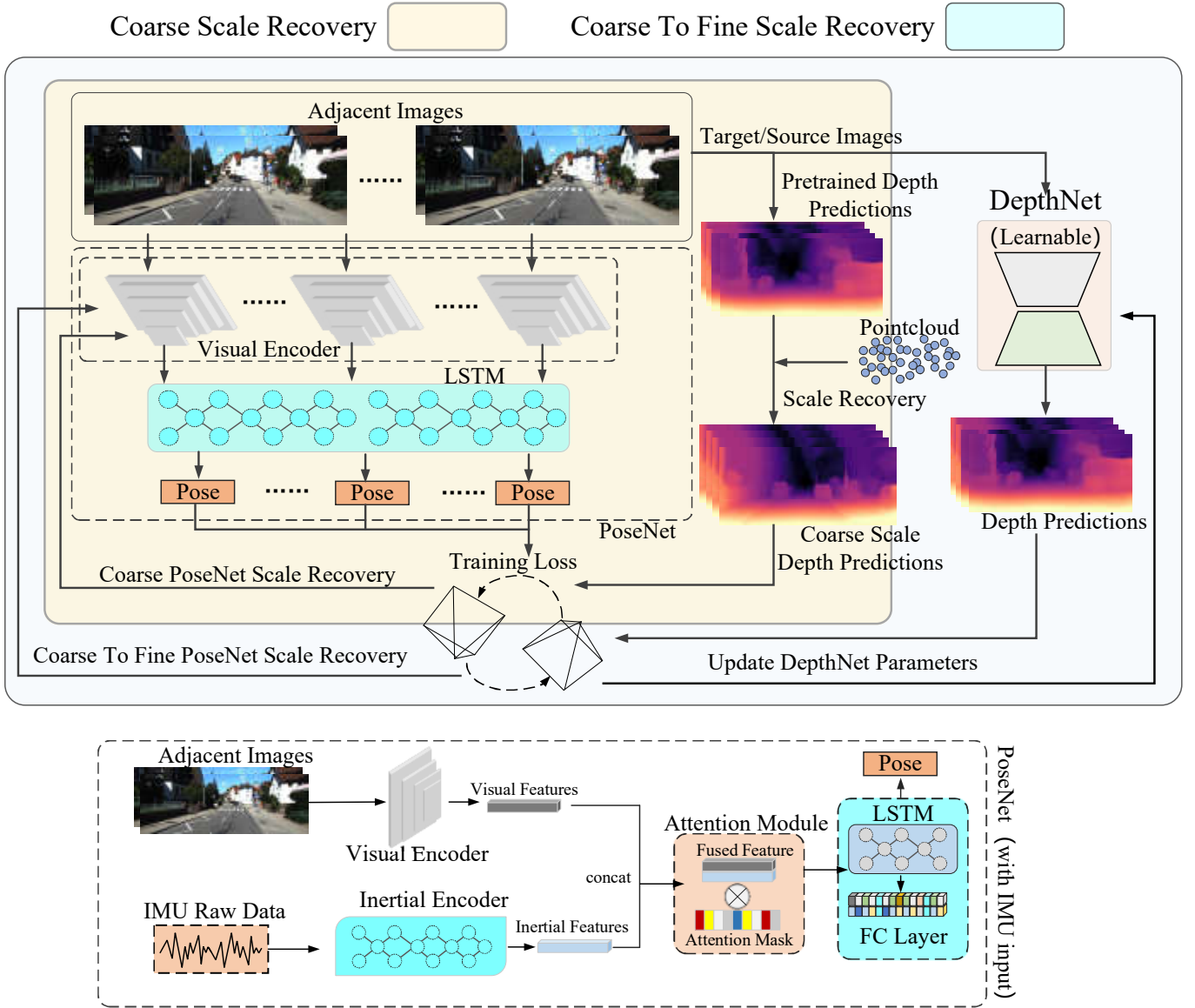


Fig. 1: overview of our framework

- Extensive experiments were conducted to validate the effectiveness of our proposed model. Our model produces pose and depth estimates robustly, even in low-light condition (i.e. a driving scene at night), a very challenging task for traditional VO/SLAM.

II. RELATED WORKS

A. Traditional Visual Odometry

Visual Odometry (egomotion estimation) is to calculate the relative pose of a moving camera through the matching feature points between different image frames via multi-view geometry model. Its main processes can be divided into: feature point extraction, feature point matching, outlier elimination, and bundle adjustment. LIBVISO [2] is a classic model-based visual odometry, that uses two different types of convolution kernels to detect the maximum response points in the image as feature points, and uses RANSAC [3] algorithm to filter the

matching feature points. PTAM [4] uses FAST [5] algorithm to detect feature points on images with different resolutions, in order to improve the performance of odometry at different scales. ORB-SLAM [6] adds stereo camera and depth camera to extend its application. In the texture-missing environment, the direct-method shows better robustness in pose estimation than feature-point based methods. DSO [7] and LSD-SLAM [8] use the corresponding pixel difference between adjacent images to construct photometric loss model to calculate camera pose. Under low-light environments, the performance of visual odometry decreases due to the failure of feature detection and matching. Combined IMU with camera, visual-inertial odometry (VIO) obtains better robustness and higher accuracy in pose estimation. [9] uses IMU pre-integration to integrate IMU raw data and optimizes the re-projection loss using matching feature points and point clouds. VINS [10] adds automatic initialization, relocation, loop closure detection and other functions to form a more complete visual-inertial

odometry.

B. The supervised learning of ego-estimation estimation

DeepVO [11] is a representative work of end-to-end learning based visual odometry (VO). It uses the convolution layers of FlowNet [12] as the visual feature extractor, and a LSTM [13] network to integrate the visual features of multiple images. Fully-connected layers are added after the LSTM network to transform features into pose predictions. Leveraging high-accuracy pose labels to train the model, DeepVO can learn to predict absolute pose predictions. [14] uses the LSTM network to process inertial data to obtain the motion features from a sequence of inertial data. It combines the visual features and inertial features to form the fused features. [15] adds an attention module into the visual-inertial odometry network to improve the robustness, and shows better performance in multiple complex environments. [16] introduces to fuse point clouds with inertial information to form a multi-sensor odometry estimation network. [17] introduces a memory and refining module that preserves important contextual information and based on that further improves poses. DAVO [18] improves the performance of supervised learning based VO by fusing the inputs from semantic segmentation, optical flow and RGB image via an attention module.

C. The Unsupervised learning of ego-estimation estimation

Unsupervised learning of egomotion methods have attracted attention, as they do not require high-precision pose labels. SfMLearner [19] designs a double network structure: PoseNet and DepthNet. It takes three consecutive images as the optimization sequence. PoseNet is responsible for estimating the relative pose between each two images. DepthNet is responsible for predicting the target frame depth. It combines relative pose estimates, target depth prediction and target/source images pixels to construct the photometric loss. In order to improve the accuracy of depth prediction, DepthNet adopts U-Net [20] like structure, which connects the multi-scale feature map of decoder and encoder. [21] uses ResNet18 [22] as the backbone of PoseNet and DepthNet. In order to obtain a more accurate pose and depth estimate, it upsamples different resolution depth predictions from DepthNet decoder to raw image resolution. And then it combines multi-scale depth predictions to form photometric loss. Besides, it adds the per-pixel minimum reprojection loss to eliminate the outliers in the photometric loss. [23] predicts disparity map at all scales in DepthNet encoder and decoder, and it transforms disparity maps into pseudo-labels. It uses pseudo-labels as self-distillation signals in training process. Meanwhile, it introduces depth hint labels into the photometric loss to facilitate depth learning. To avoid overfitting, it also proposes a data augmentation method for depth estimation. In order to solve the problem of inconsistent depth prediction scales, [24] proposes a depth scale consistency loss to constrain the depth and pose estimate to a unified scale. After multiple training iterations, the depth prediction in whole training set will keep a global consistent scale metric. [25] designs a separate scale-net to predict the scale of each depth map. In order to obtain the pose and depth

with absolute scale, PackNet-SfM [26] introduces instantaneous velocity to calculate the adjacent frames displacement as weak velocity supervision. PackNet-SfM combines weak velocity supervision with the relative displacement estimate from PoseNet to construct velocity supervision loss. In order to introduce IMU data into unsupervised work, VIOlearner [1] used CNN to process IMU data and designed online error correction module to calculate multi-scale photometric errors. They interpolate the sparse point clouds to ground truth depth labels, and then they integrate the depth labels in photometric error with adjacent images. The performance of odometry is better than that of end-to-end ViNet, but this work does not include depth estimation, so it can not reconstruct the scene in whole trajectory. Self-VIO [27] transforms IMU data into inertial features through CNN and combines them with visual features to obtain fusion features. A fusion selection module is built to filter fusion features, and a GAN [28] discriminator is designed to optimize the depth prediction to obtain high-frequency structure. At the same time, LSTM network is also used to comprehensively optimize the multi frame pose and depth predictions, Experimental results show that the performance of the proposed VIO is comparable to that of the mainstream model-based VIO. UnVIO [29] introduces two optimization modules: intra-window optimization and inter-window optimization. It constructs the photometric error between two adjacent frames and smooth loss in intra window optimization. In inter window optimization, integrated information and pose prediction of odometry are used to construct trajectory consistency loss and 3D geometric consistency loss. Two kinds of consistency loss can constrain the global pose scale, and make pose prediction more consistent. However, the network cannot obtain pose results with absolute scale.

III. SELF-SUPERVISED VISUAL EGOMOTION AND DEPTH LEARNING

A. Framework

The overview framework of our proposed self-supervised ego-motion and depth learning is shown in Figure 1. Inspired by [19], our framework also adopt double network design: PoseNet and DepthNet. Our PoseNet includes visual encoder, inertial encoder, attention based feature fusion module and pose estimation module. The framework inputs a sequence of images, and outputs the corresponding poses and depth maps. A pair of adjacent images are feed into ResNet18 based visual feature encoder to extract multi-state visual features, after which a LSTM network is used to model their temporal dependency. The visual features after LSTM are input into fully connected layers (FC layers) to produce the relative pose between the target frame and the source frame. DepthNet estimates the depth of each image in the image sequence. In addition, inertial data can be introduced into the framework to formulate visual-inertial PoseNet. Inertial feature extractor encodes inertial features from a sequence of IMUs. Then, an attention module is used to combine visual features and inertial features, which are further feed into LSTM. Our framework is trained in two steps: 1.Coarse Scale Recovery, it makes the PoseNet output pose with coarse absolute scale. 2. Coarse To

Fine Scale Recovery, it refines the PoseNet pose prediction and updates the DepthNet parameters.

1) *Visual Encoder*: We use ResNet18 backbone as the visual feature encoder f_{visual} . Two adjacent images $\{\mathbf{I}_i, \mathbf{I}_{i+1}\}$ are combined on the RGB channel to obtain 6-dimensional tensors, which are inputted into the visual feature encoder to obtain visual features in 1/4 input image size. In order to simplify the network structure and improve the forward efficiency, we use global average pooling to transform ith frame visual features into a 128 dimensional feature vector \mathbf{v}_i .

$$\mathbf{v}_i = f_{\text{visual}}\{\mathbf{I}_i, \mathbf{I}_{i+1}\} \quad (1)$$

2) *Inertial Encoder*: The data acquisition frequency of IMU is higher than that of camera, and it has high measurement accuracy in a short time. Between two adjacent images $\{\mathbf{I}_i, \mathbf{I}_{i+1}\}$, there exist j imu raw data $M_{i \rightarrow i+1}^{0 \dots j-1}$. The j th imu frame includes linear acceleration α_j and angular velocity ω_j in body coordinate, is one-dimensional time series data, so we introduce the Bi-directional LSTM network as inertial feature encoder f_{inertial} , which excels at processing time series data. The input dimension of two-layer Bi-directional LSTM network is 6, the number of hidden state $\{\mathcal{H}_{j-1}, \mathcal{H}_j\}$ is 128, and the dimension of j th frame output inertial feature vector \mathbf{a}_j is 256.

$$\mathbf{M}_{i \rightarrow i+1} = \begin{bmatrix} \alpha_i^0 & \omega_i^0 \\ \vdots & \vdots \\ \alpha_{i+1}^{j-1} & \omega_{i+1}^{j-1} \end{bmatrix} \in \mathbb{R}^{j \times 6} \quad (2)$$

$$\mathbf{a}_i, \mathcal{H}_i = f_{\text{inertial}}\{(\alpha_i, \omega_i); \mathcal{H}_{i-1}\} \quad (3)$$

3) *Attention based Feature Fusion Module*: There may be a few misalignment in the raw data, bias in the IMU data, and errors in the calibration of intrinsics and extrinsics parameters. If the features of the two kind of data are directly combined, the odometry performance is likely to be suboptimal. Even in the pure visual feature, image features with missing texture will weaken the performance of pose estimation. Inspired by [15], we introduce the attention module in PoseNet. Therefore, poseNet can focus more on features that are conducive to improving the performance of pose estimation. We concatenate two kind of features $\{\mathbf{a}_i; \mathbf{v}_i\}$ to form the concatenated features. And then we use the attention mask [15] to filter the concatenated features. In the end we obtain the filtered fusion features \mathbf{z}_i .

$$\mathbf{z}_i = f_{\text{attention}}\{\mathbf{a}_i; \mathbf{v}_i\} \quad (4)$$

4) *Pose Estimation Module*: The filtered fusion features are brought into pose estimation module. In this module, there exist a LSTM network and a FC layer. The LSTM network integrates the filtered multi fusion features $\mathbf{z}_i, i \in 0 \dots n-1$ in one sequence window, sequence length is n . We set the hidden layer nodes in LSTM network to 1024 and the high-level output features $\bar{\mathbf{z}}_i$ dimension to 2048. After the LSTM network, we use a dropout layer with a coefficient of 0.2 to further prevent the possibility of over-fitting. We subsequently

send the high-level output features to the FC layer to obtain 6-DOF relative poses \mathbf{T}_i^{i+1} .

$$\bar{\mathbf{z}}_i = \text{LSTM}\{\mathbf{z}_i\}_{i \in 0 \dots n-1} \quad (5)$$

$$\mathbf{T}_i^{i+1} = \text{FC}\{\bar{\mathbf{z}}_i\}_{i \in 0 \dots n-1} \quad (6)$$

5) *DepthNet*: We use U-Net like DepthNet, which is divided into encoder and decoder. The encoder of the DepthNet adopts the ResNet18 backbone, which is pretrained on ImageNet data set. DepthNet encoder can extract the visual feature in input image. The decoder of the DepthNet combines the feature maps from multi-scale encoder layers. There exist multiple convolution layers and nearest neighbor interpolations in DepthNet decoder. Therefore, DepthNet decoder can upsample the visual feature to original image resolution. We take the DepthNet decoder output as the disparity map. In the end we use the reciprocal of the disparity map as the depth prediction.

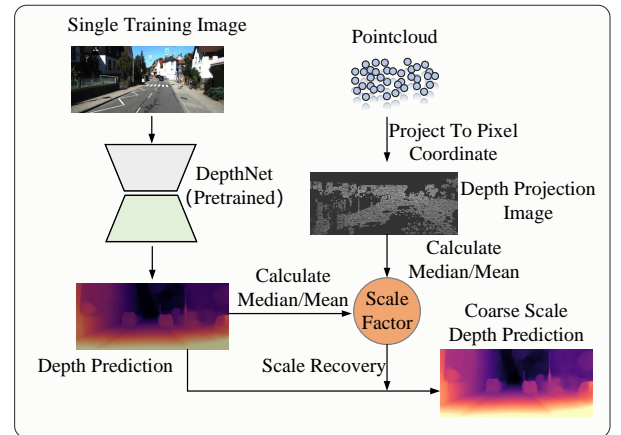


Fig. 2: coarse depth scale recovery

6) *Photometric loss*: The pixel points of the same 3D projection in two adjacent frames have brightness constancy and spatial smoothness. Given the estimated relative pose between the target frame \mathbf{I}_t and the source frame \mathbf{I}_s , the depth of target frame \mathbf{D}_t and camera intrinsic \mathbf{K} , we can generate the synthesized image $\hat{\mathbf{I}}_s$ by warping \mathbf{I}_s into target-view:

$$\mathbf{p}_s \sim \mathbf{K} \mathbf{T}_t^s \mathbf{D}_t(\mathbf{p}_t) \mathbf{K}^{-1} \mathbf{p}_t, \quad (7)$$

where \mathbf{p}_s and \mathbf{p}_t indicate pixel point in source frame and target frame.

This work aims to recover the scale of ego-motion and depth learning. If the odometry pose scale is not recovered, it is difficult for odometry to be applied in realistic scenes. The reasons why the monocular unsupervised odometry cannot recover the pose scale: 1. The monocular image cannot determine the absolute distance of the 3D point in the single image. 2. It is impossible to determine the scale of \mathbf{T}_t^s 's translation vector and \mathbf{D}_t only with photometric loss as a constraint.

B. Coarse Depth Scale Recovery via Photometric-loss-consistent Pretrained Model

We firstly introduce a depth scale recovery method via photometric-loss-consistent pretrained model. Unlike previous works [1] [30], we do not use dense depth completion results as supervisions. This is due to the fact that the performance of depth completion is closely related to the point clouds density. If point clouds are too sparse, its performance will be degraded. The dense depth completion methods can be divided into interpolation-based and learning-based methods. [1] completes the sparse point clouds by interpolation. However, the interpolated areas do not necessarily conform to the multi-view geometry, and thus the generated depths are not suitable to being applied in learning depth recovery. The learning-based methods [30], [31] learn to generate dense depths from sparse depths, which can mitigate such problems to some extent, but there still exist completion areas that do not conform to multi-view geometry, such as out of the LIDAR scanning range. And it is too complicated to remove outliers before introducing these completion-based depths as supervisions into photometric loss for scale recovery.

To handle the problem mentioned above, in our framework, we propose to use a pre-trained DepthNet to produce the depth predictions, and the scale of depth prediction is recovered by comparing them with the corresponding point clouds. The depth predictions from pre-trained model naturally conform to the multi-view geometry. The depth predictions from DepthNet are more smooth and complete, and there is no need to remove abnormal values in advance. We use the scale-recovered depth prediction as the supervisions for the recovery of pose and depth estimates.

We firstly transform the point cloud vector $\mathbf{v}_{4 \times 1}$ from LIDAR to the pixel coordinate as the depth projection point \mathbf{d}_v .

$$\mathbf{d}_v = \mathbf{P}_{c2} \mathbf{T}_{c0}^{\text{rect}} \mathbf{T}_v^{c0} \mathbf{v}_{4 \times 1} \quad (8)$$

where \mathbf{P}_{c2} is projection matrix, $\mathbf{T}_{c0}^{\text{rect}}$ is transformation matrix from camera $c0$ coordination to rectified camera $c0$ coordination, \mathbf{T}_v^{c0} is transformation matrix from lidar \mathbf{v} coordination to camera $c0$ coordination. We form the depth projection image \mathbf{D}_v from depth projection points \mathbf{d}_v .

Then we calculate the ratio between the median/mean value of depth projection images $\text{med}(\mathbf{D}_v)$ and the median/mean value of depth predictions from pre-trained DepthNet $\text{med}(\mathbf{D}_t)$. The scale factor ε is calculated as below,

$$\varepsilon = \frac{\text{med}(\mathbf{D}_v)}{\text{med}(\mathbf{D}_t)} \quad (9)$$

Finally, the scale factor ε is multiplied with the depth predictions to obtain the depths with absolute scale $\bar{\mathbf{D}}$.

$$\bar{\mathbf{D}} = \varepsilon \cdot \mathbf{D} \quad (10)$$

C. Single-directional Coarse Pose Scale Recovery

The depths with absolute scale are further leveraged to recover the pose scale of our self-supervised learning framework. We propose a two-stages process to achieve this. The first stage

aims to estimate coarse poses by exploiting the calculated coarse depths, and then the second stage refines the network estimates by jointly optimizing poses and depths.

Firstly, coarse poses are obtained by integrating the calculated coarse depths from Equation 10 into the Equation 7 to produce the synthesized images $\hat{\mathbf{I}}_s$ in target frame. We calculate the difference between the wrapped images $\hat{\mathbf{I}}_s$ and the real image in target frame \mathbf{I}_t to construct a photometric loss. Besides, SSIM loss is added to mitigate complex illumination changes [32]. We formulate our photometric loss $\mathcal{L}_{\text{photo}}$ as below,

$$\mathcal{L}_{\text{photo}} = \lambda_1 \cdot |\mathbf{I}_t - \hat{\mathbf{I}}_s| + \lambda_2 \cdot \frac{1 - \text{SSIM}(\mathbf{I}_t, \hat{\mathbf{I}}_s)}{2}, \quad (11)$$

where λ_1 and λ_2 are set as 0.15 and 0.85. The specific function of SSIM can refer to [32]. (please add SSIM function)

To encourage pose and depth predictions to be scale consistent, a 3D geometric consistency loss \mathcal{L}_{GC} [24] is introduced:

$$\mathcal{L}_{\text{GC}} = \frac{|\hat{\mathbf{D}}_s - \mathbf{T}_t^s \mathbf{D}_t|}{\hat{\mathbf{D}}_s + \mathbf{T}_t^s \mathbf{D}_t}, \quad (12)$$

where $\mathbf{T}_t^s \mathbf{D}_t$ indicates the process of wrapping the target depth \mathbf{D}_t into the source frame view using the relative pose \mathbf{T}_t^s . And $\hat{\mathbf{D}}_s$ is the interpolated source depth map aligning with $\mathbf{T}_t^s \mathbf{D}_t$.

Most existing unsupervised ego-motion networks optimize the learned pose and depth between adjacent frames. To consider the temporal dependency of poses and depths in consecutive frames, our framework optimizes them in a sequence window, which further encourages the pose scale-recovery to be more smooth in a larger window size. We set i as the time step of the target frame, $i+1$ as the time step of source frame, and n as the sequence window length. In each time step, we combine photometric loss $\mathcal{L}_{\text{photo}}^i$ and 3D geometric consistency loss $\mathcal{L}_{\text{GC}}^i$ to form an optimization loss. Combining the total losses of n frames, we form the single direction scale-recovery loss $\mathcal{L}^{i \rightarrow i+1, i \in n}$ as below,

$$\mathcal{L}_{\text{forward}}^{i \rightarrow i+1} = \lambda_3 \cdot \sum_{i=1}^n \mathcal{L}_{\text{photo}}^i + \lambda_4 \cdot \sum_{i=1}^n \mathcal{L}_{\text{GC}}^i \quad (13)$$

where λ_3 and λ_4 are set as 1 and 0.5.

We use the calculated coarse depths $(\bar{\mathbf{D}}_t, \bar{\mathbf{D}}_s)$ as the target and source depth in this stage to construct a coarse scale recovery loss $\mathcal{L}_{\text{coarse}}$,

$$\mathcal{L}_{\text{coarse}} = \mathcal{L}_{\text{forward}}^{i \rightarrow i+1} |(\bar{\mathbf{D}}_t, \bar{\mathbf{D}}_s) \quad (14)$$

The model is trained for several epochs to obtain a coarse scale recovered PoseNet, and then the entire framework is further refined in the next stage for jointly optimizing PoseNet and DepthNet together.

D. Bi-directional Coarse-to-Fine Pose Scale Recovery

In the coarse scale recovery stage, the depths are calculated from pre-trained model and estimated scale factor. This stage considers to enable pose and depth learning jointly, which further refines pose and depth estimates.

Instead of using calculated depths, we use the depth predictions from DepthNet as the target and source depths to

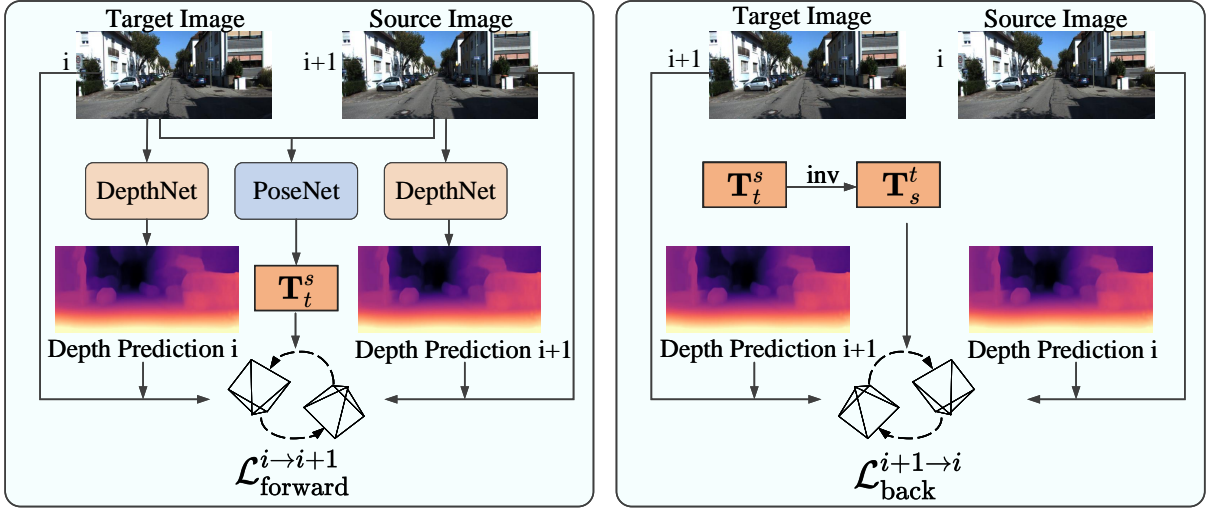


Fig. 3: The calculation of forward loss and backward loss

construct the photometric loss and 3D geometry consistency loss of coarse-to-fine scale recovery. If the optimization is only on the forward-direction, the model encourages depth predictions to be overfit on one side, leading to unstable training. Therefore, we introduce a backward loss,

$$\mathcal{L}_{\text{back}}^{i+1 \rightarrow i} = \lambda_3 \cdot \sum_{i=1}^n \mathcal{L}_{\text{pho}}^i + \lambda_4 \cdot \sum_{i=1}^n \mathcal{L}_{\text{GC}}^i \quad (15)$$

Here, as shown in Figure 3, the relative pose and the order of target and source frame are inverse.

Furthermore, we introduce an edge-aware smoothness loss $\mathcal{L}_{\text{smooth}}$ to overcome the shortage of photometric loss in the low-texture regions [33].

$$\mathcal{L}_{\text{smooth}} = \sum_{p \in (u,v)} (e^{-\nabla \mathbf{I}_t(p)} \cdot \mathbf{D}_t(p))^2 \quad (16)$$

where p indicates pixel point in coordination (u, v) , and $\mathbf{I}_t(p)$ indicates the pixel value in target frame \mathbf{I}_t , ∇ means the first derivative along two spatial directions on pixel coordination (u, v) .

Combining the forward $\mathcal{L}^{i \rightarrow i+1}$ loss, backward $\mathcal{L}^{i+1 \rightarrow i}$ loss and smoothness loss $\mathcal{L}_{\text{smooth}}$, the total loss for bi-directional scale recovery is formulated as:

$$\mathcal{L}_{\text{refine}} = \lambda_5 (\mathcal{L}_{\text{forward}}^{i \rightarrow i+1} + \mathcal{L}_{\text{back}}^{i+1 \rightarrow i})|_{(\mathbf{D}_t, \mathbf{D}_s)} + \lambda_6 \cdot \mathcal{L}_{\text{smooth}} \quad (17)$$

where we set $\lambda_5 = 1$ and $\lambda_6 = 0.1$. $(\mathbf{D}_t, \mathbf{D}_s)$ are the learned depth from DepthNet.

E. Discussion

We have also tried to use coarse scaled depth predictions to directly train the overall framework, instead of dividing training process into two stages: coarse scale recovery and coarse to fine scale recovery. However, the experimental results show that the pose and depth scale cannot be recovered directly by introducing depth labels. We analyze that since the absolute-scale depth supervisions are non-learnable, at the beginning of training, the photometric loss formed by the depth

supervision is large, and the loss reduction potential is small. The photometric loss formed by the learnable depth prediction will decrease with the training iteration, and the loss reduction potential is large. Besides, the direction of network training is consistent with the direction of loss reduction. Therefore, the scaled depth supervision can not help framework to recover absolute scale in direct training.

IV. EXPERIMENT

This section introduces implementation details, and discusses the evaluation of pose and depth estimation of our proposed model above two datasets. In addition, ablation study is conducted to verify the effectiveness of the important modules in our model.

A. Training details

We use PyTorch to implement our proposed network. Our model is trained and tested via a NVIDIA RTX3090 GPU. Adam is chosen as optimizer to recover the optimal parameters, whose attenuation coefficient is $\beta_1 = 0.9$, $\beta_2 = 0.999$. The model is trained for 200 epochs, and in each epoch there are 1000 random data sequences. The model training follows a two-stages process: first, we use the pseudo depth labels to train the network for around 30-100 epochs, until a coarse pose estimation with absolute scale can be recovered; then, depth and pose networks are jointly trained to enable coarse-to-fine pose and depth estimation. The learning rate is chose as $1e-4$ in the first stage and reduced to $1e-5$ in the second stage.

B. Datasets

1) *KITTI Odometry Dataset*: The KITTI Raw dataset is a typical car-driving dataset. It provides RGB images, IMU, LIDAR point cloud data and ground-truth pose data. We use this dataset to generate pseudo depth labels and odometry network training data. The KITTI Raw dataset for odometry includes 10 sequences. We use Sequence 00-08 excluding Sequence 03 for training and evaluation, as the IMU data of

TABLE I: The pose performance on the KITTI dataset, "Scale" indicates whether the pose estimates are scaled or not.

Method	Sensors	Scale	Seq. 09		Seq. 10		Avg	
			t_{rel}	r_{rel}	t_{rel}	r_{rel}	t_{rel}	r_{rel}
ORB-SLAM	Mono	x	15.3	0.26	3.68	0.48	9.49	0.37
Depth-VO-Feat	Stereo	x	11.92	3.60	12.62	3.43	12.27	3.515
GeoNet	Mono	x	23.94	9.81	20.73	9.10	22.34	9.46
Monodepth2	Mono	x	18.12	3.86	12	5.34	15.06	4.6
SfMLearner	Mono	x	17.84	6.78	37.91	17.78	27.875	12.28
SC	Mono	x	8.62	3.05	7.81	4.9	8.22	3.98
Ours(VO)	Mono	✓	7.90	1.23	6.55	2.05	7.23	1.64
VINS	Mono+IMU	✓	41.47	2.41	20.35	2.73	30.91	2.57
VINet	Mono+IMU	✓	11.83	3.00	8.60	4.39	10.22	3.70
UnVIO	Mono+IMU	x	4.41	0.92	6.42	0.63	5.41	1.55
Ours(VIO)	Mono+IMU	✓	5.48	0.19	5.37	0.43	5.43	0.31
Ours(VIO) (Scaled)	Mono+IMU	✓	3.65	0.19	4.42	0.43	4.04	0.31

Sequence 03 are missing, while Sequence 09 and 10 are used for testing. Since the IMU and LIDAR data in the KITTI Raw dataset are unsynchronized, we manually synchronize these data according to their timestamps. The frequency of IMU is 100Hz, while the frequency of images and the synchronized LIDAR point cloud data is 10Hz. The ground-truth pose is not involved in training process, but used in the testing process to evaluate the pose accuracy.

2) *MVSEC Dataset*: In order to evaluate our model performance at night, we select the Multi Vehicle Stereo Event Camera (MVSEC) dataset, which collected gray images and IMU data. The images were sampled at a frequency of 20Hz and IMU data were recorded at a frequency of 200Hz. In our experiments, we use the data from several car-driving scenarios in daytime and at night, including two day-time sequences (Day1, Day2) and three night-time sequences (Evening1, Evening2, Evening3). We used the Day1, Day2, Evening1, and Evening2 as training data, and the Evening3 as testing data. From the figure 4, it can be seen that the lighting conditions at night impose challenges to the visual pose and depth estimation. The dataset also provides ground-truth pose, which is only used in the testing process for evaluation.

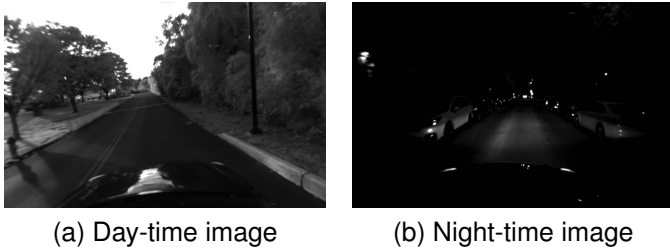


Fig. 4: The sample images of the MVSEC dataset: a) driving in daytime b) driving at night

C. Pose evaluation on the KITTI dataset

We first come to evaluate our proposed VO/VIO models on the public-available KITTI dataset. Following the previous research, we use Sequence 00-08 for training and evaluation,

and Sequence 09 and 10 for testing. The KITTI's official evaluation is adopted here. It is to calculate the RMSE of translation vector and rotation of the sequences with a length from 100m to 800m, and average them as the criterion of pose accuracy.

For vision only pose estimation, we compare with a mainstream traditional SLAM (i.e. ORB-SLAM) and five learning based VOs (i.e. Depth-VO-Feat, GeoNet, MonoDepth2, SfMLearner, SC). Among the learning based baselines, Depth-VO, GeoNet, MonoDepth2, SfMLearner are scale-ambiguity, while SC is scale-consistent, but still loses its absolute scale. However, our proposed self-supervised VO can produce pose with global scale. From Table I, it is clear to see that our model outperforms all both traditional and learning based baselines in translation, and outperforms all the learning based VOs in rotation. Our VO model further improves SC 12.04% in translation and 58.79% in rotation averagely. Though the rotation estimation of ORB-SLAM is still better than our VO model slightly, we show that by introducing inertial data into our model as learning based VIO, our VIO model shows superior performance in rotation than all the VO/VIO baselines.

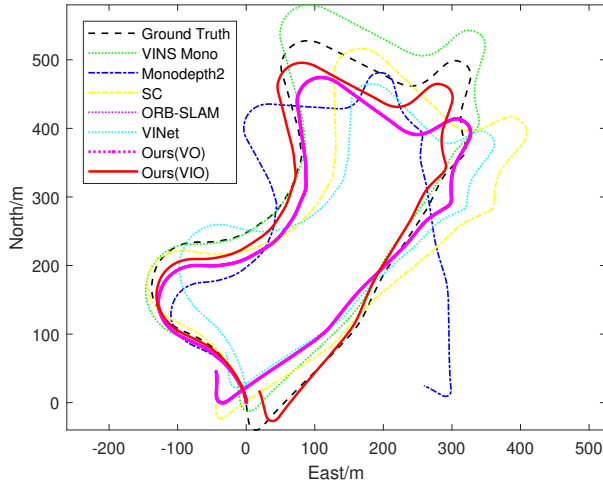
Our VIO model is compared with a representative traditional VIO, i.e. VINS, and two learning based VIO, i.e. VINet and UnVIO. VINet is a supervised learning based VIO model using a combination of ConvNet and LSTM. UnVIO is an unsupervised learning based VIO model via novel view synthesis similar to our model, but it has no absolute scale metric. Clearly, our model significantly outperforms these baselines in both translation and rotation. Our VIO model improves the translation and rotation estimation of UnVIO around 25.32% and 80% respectively. As illustrated in Figure 5, the generated trajectories from our VO and VIO models are closer to the ground-truth trajectories, compared with other baselines, i.e. VINS-mono, MonoDepth2, SC, ORB-SLAM and VINet.

D. Depth evaluation on the KITTI Dataset

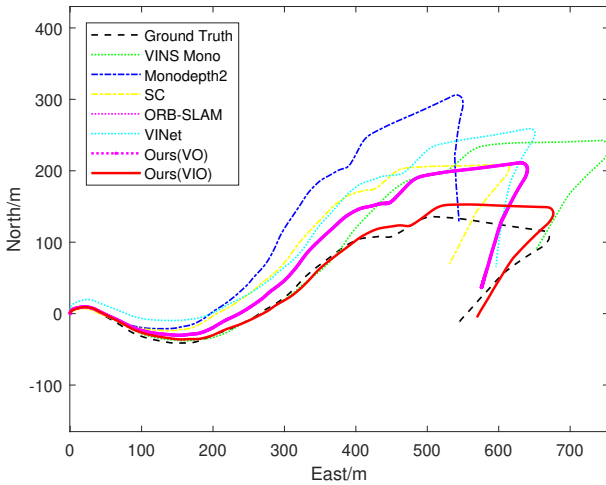
In addition to pose estimation, we also evaluate the depth evaluation on the KITTI dataset. Different from the SC-SfMLearner that use KITTI raw dataset for training, we use

TABLE II: The depth evaluation on the KITTI dataset. These models are trained with Sequence 00-08, and tested with Sequence 09 and 10.

Method	Sensors	Resolution	Scale	Error metric			Accuracy metric(δ)		
				Abs Rel \downarrow	Sq Rel \downarrow	RMSE \downarrow	(1.25) \uparrow	(1.25 ²) \uparrow	(1.25 ³) \uparrow
SfMLearner	Mono	832 \times 256	x	0.3272	3.1131	9.5216	0.4232	0.7010	0.8476
SC	Mono	832 \times 256	x	0.1629	0.9644	4.9129	0.7760	0.9315	0.9773
UnVIO	Mono+IMU	832 \times 256	x	0.1322	0.73005	4.2443	0.8324	0.9509	0.9821
Ours1	Mono	832 \times 256	x	0.1322	0.7244	4.2715	0.8313	0.9498	0.9816
Ours2	Mono	832 \times 256	\checkmark	0.1308	0.6980	4.2930	0.8318	0.9520	0.9836
Ours3	Mono+IMU	832 \times 256	\checkmark	0.1301	0.6942	4.2963	0.8341	0.9526	0.9837



(a) KITTI Sequence 09



(b) KITTI Sequence 10

Fig. 5: The trajectories of our proposed self-learning based VO and VIO model on Sequence 09 and 10 of the KITTI dataset, comparing with baselines.

Sequence 00-08 of KITTI as these sequences are with IMU data. Table II shows the quantitative results of the depth estimation from our proposed models on the Sequence 09 and

10, comparing with three mainstream learning based depth estimation methods, i.e. SfMLearner, SC and UnVIO.

In Table II, we use following evaluation metrics for depth estimation, where p indicates pixel point in coordination (u, v) , \mathbf{D} and \mathbf{D}_v indicate learned depth prediction from DepthNet and corresponding depth projection image. a is the threshold factor. N is the sum of pixel points in the depth image coordinate.

$$\begin{aligned}
 \text{Abs Rel} &= \frac{1}{N} \sum_p \frac{|\mathbf{D}(p) - \mathbf{D}_v(p)|}{\mathbf{D}_v(p)} \\
 \text{Sq Rel} &= \frac{1}{N} \sum_p \frac{(\mathbf{D}(p) - \mathbf{D}_v(p))^2}{\mathbf{D}_v(p)} \\
 \text{RMSE} &= \sqrt{\frac{1}{N} \sum_p (\mathbf{D}(p) - \mathbf{D}_v(p))^2} \\
 \delta(a) &= \frac{1}{N} \sum_p \max\left(\frac{\mathbf{D}_v(p)}{\mathbf{D}(p)}, \frac{\mathbf{D}(p)}{\mathbf{D}_v(p)}\right) < a
 \end{aligned} \tag{18}$$

It indicates that our depth estimation models (Ours2 and Ours3) can produce depth in absolute scale and outperform other three baselines. The introduction of IMU into depth estimation throws little influence upon depth estimation. Figure 6 shows several depth images from monocular camera, generated by our proposed models and baselines. We can see that compared with other learning based depth estimation models, our models can produce depth maps with more delicate details, e.g., the poles can be clearly shown in our depth maps.

TABLE III: A comparison of the scale factor estimation with or without our introduce scale recovery method.

Method	Scale	μ	δ
Ours	x	33.109	4.384
Ours	\checkmark	1.128	0.118

Moreover, we continue to study the effectiveness of our introduced scale recovery method. Table III shows the mean value and standard deviation value by comparing the scale factor of depth estimation with or without scale recovery. It can be seen that the averaged scale coefficient of depth estimation values is closer to 1 when adopted our proposed coarse-to-fine scale recovery method. If scale recovery is not performed, there is a large distance between the estimated

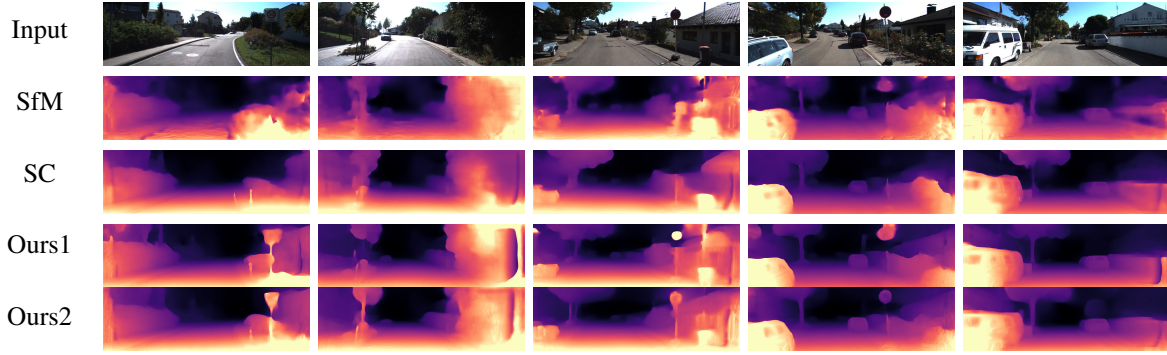


Fig. 6: The samples of depth estimation from SfM-Learner, SC and our proposed models

scale-ambiguous depths and real depths. This indicates that the introduction of scale recovery can not only enable PoseNet to output pose predictions with global absolute scale, but also help DepthNet output depth estimates closer to the real absolute scale metric.

E. Pose and Depth Evaluation on the Night Scenes of MVSEC Dataset

To evaluate our proposed model on very challenging night scenes, which are in low-light conditions and relatively featureless, we selected the MVSEC dataset to conduct experiments. A recent state-of-the-art monocular SLAM, (i.e. ORB-SLAM3), a representative unsupervised-learning based VO (i.e. SC-SfMLearner) and a supervised learning based (i.e. DeepVO) are chosen for a comparison.

The trajectories of each model on Evening3 are displayed in Figure 7. It can be seen that the learning based VOs can robustly estimate vehicle ego-motion and generate trajectories in this challenging scene. However, the traditional model, ORB-SLAM3-Mono fails. This might be due to fact that ORB-SLAM3 Mono can extract and match enough feature points under low-light environment, and thus are not capable of performing effective feature tracking for pose estimation, leading to positioning failure. In contrast, deep learning networks excel at learning and extracting features and thus enable learning-based methods to extract sufficient and reliable visual feature for positioning.

We use RMSE as the evaluation metric via Equation 19, and further compare these quantitative results in Table IV,

$$\text{Error} = \sqrt{\frac{1}{n}(\mathbf{x}_i - \mathbf{x}_i^{\text{gt}})^2} \quad (19)$$

Where \mathbf{x}_i represents the estimated three-dimensional location in i th frame, and \mathbf{x}_i^{gt} is the corresponding ground-truth location. The quantitative results show that the performance of our proposed VO model exceeds both unsupervised learning based VO, i.e. SC, and supervised learning based VO, i.e. DeepVO. It demonstrates that our framework can robustly and accurately estimate pose in low light environment.

In addition, we qualitatively evaluate the depth estimation performance of our framework in the challenging night scene, comparing with SC. Figure 8 shows input RGB image, depth maps from LIDAR data, depth estimation from SC, and depth

TABLE IV: The pose estimation results in the night car-driving scenes.

Method	Sensors	Scale	Error
ORB-SLAM3 Mono	Mono	✓	failed
SC-SfMLearner	Mono	x	72.05
DeepVO	Mono	✓	39.37
Ours(VO)	Mono	✓	35.12
Ours(VIO)	Mono+IMU	✓	19.62

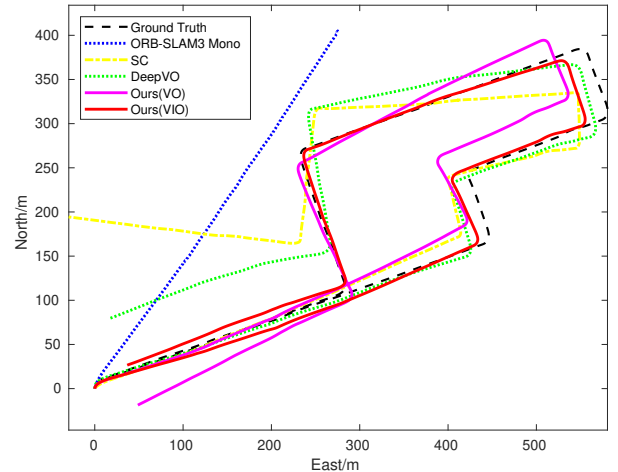


Fig. 7: The generated trajectories in the night car-driving scenes

estimation from our our model. Clearly, SC does not perform well when it is in the area of strong light. SC will misleadingly estimates depth in a shorter distance in strong-light condition. It might be because our model introduces a coarse-to-fine stage into depth estimation that enables DepthNet to overcome the influence of light condition, e.g. too strong or too dark.

F. Ablation Study

Finally, we conduct ablation study to verify the effectiveness of different modules in our framework. We use the KITTI dataset and learning based VIO model. The results of ablation

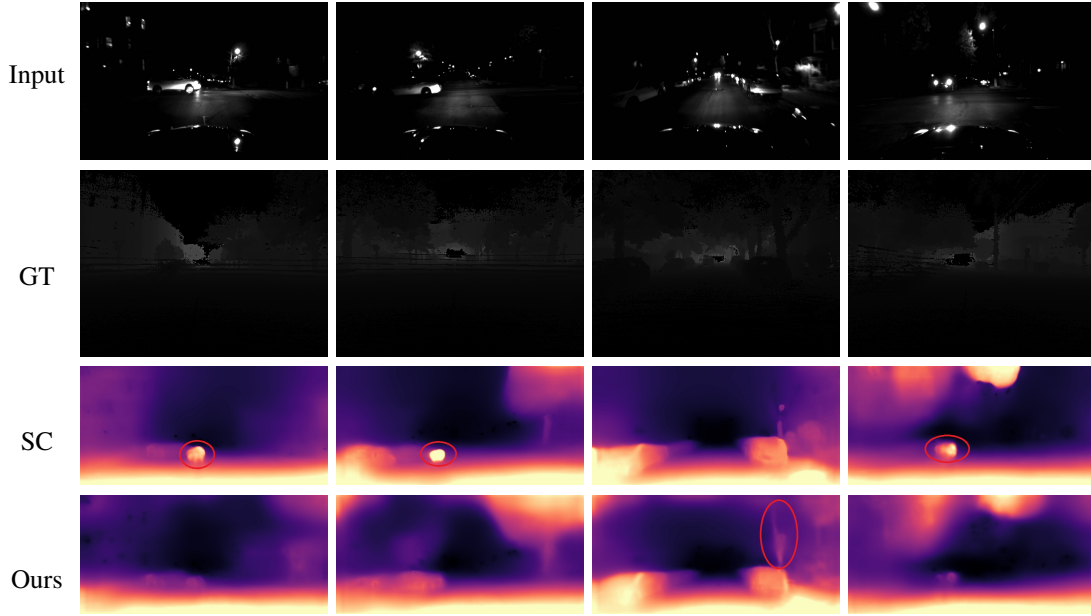


Fig. 8: The depth predictions from our model and baselines in low-light condition of driving at night.

study into framework modules are shown in Table V. In order to test the impact of the attention module on pose estimation, we remove attention mask and directly input the fusion features of vision and inertial into the subsequent LSTM and PoseNet. We can see that the attention module can further improve the performance of pose network, especially rotation estimation. Also, the addition of IMU data into framework can enhance the network performance. This indicates the effectiveness of multimodal fusion, as inertial data contributes to rotation estimation more, and the fusion of features can compensate the shortcomings of different modalities. In order to evaluate the effectiveness of LSTM network, we remove LSTM module, and input the fused features directly into PoseNet, showing that adding LSTM module enhances model performance.

TABLE V: The ablation study into framework modules

Method	IMU	LSTM	Attention	Seq.09		Seq.10		Avg	
				t_{rel}	r_{rel}	t_{rel}	r_{rel}	t_{rel}	r_{rel}
Ours		✓	✓	8.84	1.31	7.34	1.98	8.09	1.64
Ours	✓		✓	14.57	0.56	10.92	1.73	12.74	1.15
Ours	✓	✓		5.06	0.29	6.33	0.57	5.70	0.43
Ours	✓	✓	✓	5.48	0.19	5.37	0.43	5.43	0.31

Then, we study the impact of different sequence lengths on pose estimation, and the comparison results are shown in Table VI. Compared with a short sequence length (3 frames), we can see that a longer window length (a sequence of 5 frames) can improve both translation and rotation estimation accuracy, especially the rotation improve is more significant.

Finally, the influence of adding scaled depth predictions and learned depth on pose estimation is studied. The comparison results are shown in Table VII. In order to verify the effectiveness of the learnable DepthNet on pose estimation, Ours1

TABLE VI: The ablation study into sequence length

Method	Window length	Seq.09		Seq.10		Avg	
		t_{rel}	r_{rel}	t_{rel}	r_{rel}	t_{rel}	r_{rel}
Ours1	3	6.42	0.45	4.90	0.55	5.66	0.5
Ours2	5	5.48	0.19	5.37	0.43	5.43	0.31

follows coarse-to-fine scale recovery training, but it uses the scaled depth predictions instead of the learned depths from DepthNet, to form the total loss for bi-directional scale recovery, and the learning rate is consistent with Ours3. Although the scaled depth predictions must be higher in accuracy than the learned depths from DepthNet, the scaled depth predictions are unlearnable and cannot be optimized with the iteration of training. The potential for scaled pseudo depth labels to improve the pose estimation accuracy is thus limited. In order to verify the effectiveness of the learned depth from DepthNet on pose estimation, Ours2 does not introduce any supervision in framework, but directly uses learned depth to form the total loss for bi-directional scale recovery, and the learning rate is $1e-4$. It can be seen that the performance Ours3 with our proposed training strategy is higher than Ours1 and Ours2.

TABLE VII: The ablation into supervision signal and learning rate, "C" indicates Coarse Scale Recovery, "F" indicates Coarse-to-fine Scale Recovery, "D" indicates scaled depth predictions, "-" means this stage does not exist, "LR" indicates learning rate.

Method	Supervision		LR		Seq.09		Seq.10		Avg	
	C	F	C	F	t_{rel}	r_{rel}	t_{rel}	r_{rel}	t_{rel}	r_{rel}
Ours1	D	D	$1e-4$	$1e-5$	8.01	1.07	9.06	1.45	8.54	1.26
Ours2	-	x	x	$1e-4$	6.06	0.66	7.65	2.25	6.86	1.45
Ours3	D	x	$1e-4$	$1e-5$	5.48	0.19	5.37	0.43	5.43	0.31

V. CONCLUSION

In this work, we propose a self-supervised learning based depth and egomotion estimation framework with a novel coarse-to-fine scale recovery strategy. Our model can accurately and robustly output pose and depth with global scale metric, even in low-light conditions at night. We conducted extensive experiments to evaluate our model on two public datasets, i.e. KITTI and MVSEC. On both datasets, our model outperforms both traditional and learning based VOs/VIOs. Ablation study is also performed to verify the effectiveness of each module in our framework. In the future, we will attempt to exploit IMU data for scale recovery and pose estimation that further contributes to the performance improvement.

REFERENCES

- [1] E. J. Shmuel, K. Lindgren, S. Leung, and W. D. Nothwang, “Unsupervised deep visual-inertial odometry with online error correction for rgb-d imagery,” *IEEE transactions on pattern analysis and machine intelligence*, vol. 42, no. 10, pp. 2478–2493, 2019.
- [2] B. Kitt, A. Geiger, and H. Lategahn, “Visual odometry based on stereo image sequences with ransac-based outlier rejection scheme,” in *2010 IEEE Intelligent Vehicles Symposium*, 2010, pp. 486–492.
- [3] M. A. Fischler and R. C. Bolles, “Random sample consensus: A paradigm for model fitting with applications to image analysis and automated cartography,” in *Readings in Computer Vision*, M. A. Fischler and O. Firschein, Eds. San Francisco (CA): Morgan Kaufmann, 1987, pp. 726–740. [Online]. Available: <https://www.sciencedirect.com/science/article/pii/B9780080515816500702>
- [4] G. Klein and D. Murray, “Parallel tracking and mapping for small ar workspaces,” in *2007 6th IEEE and ACM International Symposium on Mixed and Augmented Reality*, 2007, pp. 225–234.
- [5] E. Rosten and T. Drummond, “Machine learning for high-speed corner detection,” vol. 3951, 07 2006.
- [6] R. Mur-Artal, J. M. M. Montiel, and J. D. Tardós, “Orb-slam: A versatile and accurate monocular slam system,” *IEEE Transactions on Robotics*, vol. 31, no. 5, pp. 1147–1163, 2015.
- [7] J. Engel, V. Koltun, and D. Cremers, “Direct sparse odometry,” *IEEE Transactions on Pattern Analysis and Machine Intelligence*, vol. 40, no. 3, pp. 611–625, 2018.
- [8] J. Engel, T. Schöps, and D. Cremers, “LSD-SLAM: Large-scale direct monocular SLAM,” in *European Conference on Computer Vision (ECCV)*, September 2014.
- [9] C. Forster, L. Carlone, F. Dellaert, and D. Scaramuzza, “On-manifold preintegration for real-time visual-inertial odometry,” *IEEE Transactions on Robotics*, vol. 33, no. 1, pp. 1–21, 2016.
- [10] T. Qin, P. Li, and S. Shen, “Vins-mono: A robust and versatile monocular visual-inertial state estimator,” *IEEE Transactions on Robotics*, vol. 34, no. 4, pp. 1004–1020, 2018.
- [11] S. Wang, R. Clark, H. Wen, and N. Trigoni, “Deepvo: Towards end-to-end visual odometry with deep recurrent convolutional neural networks,” in *2017 IEEE International Conference on Robotics and Automation (ICRA)*, 2017, pp. 2043–2050.
- [12] A. Dosovitskiy, P. Fischer, E. Ilg, P. Häusser, C. Hazirbas, V. Golkov, P. v. d. Smagt, D. Cremers, and T. Brox, “FlowNet: Learning optical flow with convolutional networks,” in *2015 IEEE International Conference on Computer Vision (ICCV)*, 2015, pp. 2758–2766.
- [13] S. Hochreiter and J. Schmidhuber, “Long short-term memory,” *Neural computation*, vol. 9, pp. 1735–80, 12 1997.
- [14] R. Clark, S. Wang, H. Wen, A. Markham, and N. Trigoni, “Vinet: Visual-inertial odometry as a sequence-to-sequence learning problem,” in *Proceedings of the AAAI Conference on Artificial Intelligence*, vol. 31, no. 1, 2017.
- [15] C. Chen, S. Rosa, Y. Miao, C. X. Lu, W. Wu, A. Markham, and N. Trigoni, “Selective sensor fusion for neural visual-inertial odometry,” in *Proceedings of the IEEE/CVF Conference on Computer Vision and Pattern Recognition*, 2019, pp. 10 542–10 551.
- [16] C. Chen, S. Rosa, C. X. Lu, B. Wang, N. Trigoni, and A. Markham, “Learning selective sensor fusion for state estimation,” *IEEE Transactions on Neural Networks and Learning Systems*, 2022.
- [17] F. Xue, X. Wang, S. Li, Q. Wang, J. Wang, and H. Zha, “Beyond tracking: Selecting memory and refining poses for deep visual odometry,” in *IEEE/CVF International Conference on Computer Vision and Pattern Recognition (CVPR)*, 2019, pp. 8575–8583.
- [18] X. Kuo, C. Liu, K. Lin, E. Luo, Y. Chen, and C. Lee, “Dynamic attention-based visual odometry,” in *The IEEE/RSJ International Conference on Intelligent Robots and Systems (IROS)*. IEEE, 2020, pp. 5753–5760.
- [19] T. Zhou, M. Brown, N. Snavely, and D. G. Lowe, “Unsupervised learning of depth and ego-motion from video,” in *2017 IEEE Conference on Computer Vision and Pattern Recognition (CVPR)*, 2017, pp. 6612–6619.
- [20] O. Ronneberger, P. Fischer, and T. Brox, “U-net: Convolutional networks for biomedical image segmentation,” in *International Conference on Medical image computing and computer-assisted intervention*. Springer, 2015, pp. 234–241.
- [21] C. Godard, O. Mac Aodha, M. Firman, and G. J. Brostow, “Digging into self-supervised monocular depth estimation,” in *Proceedings of the IEEE/CVF International Conference on Computer Vision*, 2019, pp. 3828–3838.
- [22] K. He, X. Zhang, S. Ren, and J. Sun, “Deep residual learning for image recognition,” in *Proceedings of the IEEE conference on computer vision and pattern recognition*, 2016, pp. 770–778.
- [23] R. Peng, R. Wang, Y. Lai, L. Tang, and Y. Cai, “Excavating the potential capacity of self-supervised monocular depth estimation,” in *2021 IEEE/CVF International Conference on Computer Vision (ICCV)*, 2021, pp. 15 540–15 549.
- [24] J. Bian, Z. Li, N. Wang, H. Zhan, C. Shen, M.-M. Cheng, and I. Reid, “Unsupervised scale-consistent depth and ego-motion learning from monocular video,” *Advances in neural information processing systems*, vol. 32, 2019.
- [25] L. Wang, Y. Wang, L. Wang, Y.-W. Zhan, Y. Wang, and H. Lu, “Can scale-consistent monocular depth be learned in a self-supervised scale-invariant manner?” *2021 IEEE/CVF International Conference on Computer Vision (ICCV)*, pp. 12 707–12 716, 2021.
- [26] V. Guizilini, R. Ambrus, S. Pillai, A. Raventos, and A. Gaidon, “3d packing for self-supervised monocular depth estimation,” in *Proceedings of the IEEE/CVF Conference on Computer Vision and Pattern Recognition*, 2020, pp. 2485–2494.
- [27] Y. Almalioglu, M. Turan, M. R. U. Saputra, P. P. de Gusmão, A. Markham, and N. Trigoni, “Selfvio: Self-supervised deep monocular visual-inertial odometry and depth estimation,” *Neural Networks*, vol. 150, pp. 119–136, 2022.
- [28] A. Creswell, T. White, V. Dumoulin, K. Arulkumaran, B. Sengupta, and A. A. Bharath, “Generative adversarial networks: An overview,” *IEEE signal processing magazine*, vol. 35, no. 1, pp. 53–65, 2018.
- [29] P. Wei, G. Hua, W. Huang, F. Meng, and H. Liu, “Unsupervised monocular visual-inertial odometry network,” in *Proceedings of the Twenty-Ninth International Conference on International Joint Conferences on Artificial Intelligence*, 2021, pp. 2347–2354.
- [30] A. Wong, X. Fei, S. Tsuei, and S. Soatto, “Unsupervised depth completion from visual inertial odometry,” *IEEE Robotics and Automation Letters*, vol. 5, no. 2, pp. 1899–1906, 2020.
- [31] F. Ma, G. V. Cavalheiro, and S. Karaman, “Self-supervised sparse-to-dense: Self-supervised depth completion from lidar and monocular camera,” in *2019 International Conference on Robotics and Automation (ICRA)*. IEEE, 2019, pp. 3288–3295.
- [32] Z. Wang, A. C. Bovik, H. R. Sheikh, and E. P. Simoncelli, “Image quality assessment: from error visibility to structural similarity,” *IEEE transactions on image processing*, vol. 13, no. 4, pp. 600–612, 2004.
- [33] T. Shen, Z. Luo, L. Zhou, H. Deng, R. Zhang, T. Fang, and L. Quan, “Beyond photometric loss for self-supervised ego-motion estimation,” *2019 International Conference on Robotics and Automation (ICRA)*, pp. 6359–6365, 2019.